

Superconducting coherence peak in near-field radiative heat transfer

Wenbo Sun,¹ Zhuomin M. Zhang,² and Zubin Jacob^{1,*}

¹*Elmore Family School of Electrical and Computer Engineering,
Birck Nanotechnology Center, Purdue University, West Lafayette, Indiana 47907, USA*

²*George W. Woodruff School of Mechanical Engineering,
Georgia Institute of Technology, Atlanta, Georgia 30332, USA*

(Dated: March 11, 2025)

Enhancement and peaks in near-field radiative heat transfer (NFRHT) typically arise due to surface phonon-polaritons, plasmon-polaritons, and electromagnetic (EM) modes in structured materials. However, the role of material quantum coherence in enhancing near-field radiative heat transfer remains unexplored. Here, we unravel that NFRHT in superconductor-ferromagnetic systems displays a unique peak at the superconducting phase transition that originates from the quantum coherence of Bogoliubov quasiparticles in superconductors. Our theory takes into account evanescent EM radiation emanating from fluctuating currents comprising Cooper pairs and Bogoliubov quasiparticles in stark contrast to the current-current correlations induced by electrons in conventional materials. Our proposed NFRHT configuration exploits ferromagnetic resonance at frequencies deep inside the superconducting band gap to isolate this superconducting coherence peak. Furthermore, we reveal that Cooper pairs and Bogoliubov quasiparticles have opposite effects on near-field thermal radiation and isolate their effects on many-body radiative heat transfer near superconductors. Our proposed phenomenon can have applications for developing thermal isolators and heat sinks in superconducting circuits.

Introduction.—Near-field radiative heat transfer (NFRHT) is mediated by evanescent electromagnetic (EM) fields emitted from fluctuating current sources inside materials [1–3], and plays a crucial role in thermal energy technologies. Considerable efforts have focused on enhancing NFRHT by using plasmons, phonons, and photonic modes in metals [4–10], polar dielectrics [11–13], hyperbolic materials [14, 15], and structured materials [16–21], where the fluctuating currents are generally related to thermal motions of electrons or ions [22]. Recent research interests focused on exploring new material platforms for controlling nanoscale radiative thermal transport [23–25]. Special interest is given to phase-transition materials with more ordered electronic phases, e.g., superconductors [25–28] or charge density waves [24]. Near-field thermal radiation from these new material platforms not only exhibits unconventional behaviors important for developing energy harvesting devices, but also encodes important material information useful for building novel probes of materials [24, 29].

One fundamental difference between thermal radiation from superconductors and metals/polar dielectrics is that fluctuating currents in superconductors are carried by Cooper pairs and Bogoliubov quasiparticles (broken Cooper pairs) rather than electrons/ions [30]. Distinct from electrons in normal conductors, Cooper pairs and Bogoliubov quasiparticles exhibit intrinsic quantum coherence effects [31]. As an example, Cooper pairs are coherent superpositions of two electrons with opposite spins, while Bogoliubov quasiparticles are coherent superpositions of electrons and holes. This superconducting coherence reveals the internal structures of the BCS condensate and is crucial for understanding superconductivity.

Previous works focused on revealing the superconducting coherence effects in electrical transport [32, 33], quasiparticle scattering [34, 35], and nuclear spin relaxation [36–38]. However, the role of superconducting coherence in NFRHT remains unexplored.

Previous works about NFRHT and superconductivity focused on dielectric/normal-metal-superconductor systems and found that NFRHT is strongly suppressed by superconductivity [25–28] at the superconducting phase transition. In those systems, thermal radiation is dominated by spectrum components at frequencies comparable to or higher than the superconducting band gap [27, 28] (Fig. 1(b)). Meanwhile, superconducting coherence effects are usually connected to low-frequency response deep inside the superconducting band gap. This indicates the necessity of exploring systems with NFRHT dominated by low-frequency spectrum components to unravel superconducting coherence effects in thermal photonics.

In this Letter, we exploit the low-frequency ferromagnetic resonance in yttrium iron garnet (YIG) to reveal superconducting coherence effects in NFRHT between YIG nanoparticles and a superconducting niobium slab. We demonstrate that NFRHT in the superconductor-ferromagnet system exhibits distinctive behaviors compared to superconductor-normal-metal/dielectric systems. Specifically, we find a superconducting coherence peak that enhances NFRHT at the phase transition, which serves as the fingerprint of superconducting coherence effects. This superconducting coherence peak leads to a negative temperature dependence of NFRHT, which is not present in NFRHT between blackbodies or conventional materials. In addition, we reveal that Cooper pairs and Bogoliubov quasiparticles have opposite effects

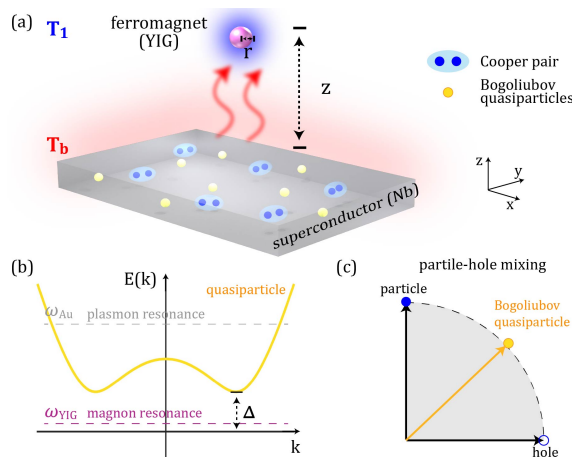


FIG. 1. (a) Design of the superconductor-ferromagnet system to unravel superconducting coherence effects in thermal photonics. (b) Energy spectra of Bogoliubov quasiparticles and superconducting band gap Δ . We exploit low-frequency YIG magnon resonance ω_{YIG} deep inside the superconducting band gap to unravel the superconducting coherence effects in NFRHT. (c) Bogoliubov quasiparticles are coherent quantum superpositions of electrons and holes, known as electron-hole mixing.

on NFRHT in this superconductor-ferromagnetic system, which can be exploited to build novel nanoscale thermal devices. Finally, we isolate the effects of Bogoliubov quasiparticles and Cooper pairs on the spatial coherence of near-field thermal radiation, and their effects on many-body NFRHT in YIG nanoparticle arrays near a superconducting slab.

Quantum coherence and Bogoliubov quasiparticles.— In superconductors, attractive interactions (e.g., phonon-mediated interactions) between electrons open a superconducting band gap Δ at the Fermi surface, leading to the formation of two unique types of particles, i.e., Cooper pairs and Bogoliubov quasiparticles [30]. As shown in Fig. 1(b), Cooper pairs are paired electrons that condense into the ground state, while Bogoliubov quasiparticles are excitations (broken Cooper pairs) separated by the superconducting band gap Δ from the ground state [31].

One unique signature of Bogoliubov quasiparticles in superconductors is their quantum nature as coherent superpositions of electrons and holes [39, 40]. This is explicitly demonstrated by the creation operator of Bogoliubov quasiparticles $a_{\mathbf{k},\sigma}^\dagger$ [31],

$$a_{\mathbf{k},\sigma}^\dagger = u_{\mathbf{k}} c_{\mathbf{k},\sigma}^\dagger + v_{\mathbf{k}} \text{sgn}(\sigma) c_{-\mathbf{k},-\sigma}, \quad (1)$$

where $c_{\mathbf{k},\sigma}^\dagger$ represents the creation of an electron with momentum \mathbf{k} and spin σ , and $c_{-\mathbf{k},-\sigma}$ represents the creation of a hole (annihilation of an electron) with momentum $-\mathbf{k}$ and spin $-\sigma$. $u_{\mathbf{k}}, v_{\mathbf{k}}$ are the coherence factors satisfying $|u_{\mathbf{k}}|^2 + |v_{\mathbf{k}}|^2 = 1$, which represent the coherent

superposition of electrons and holes for Bogoliubov quasiparticles. These coherence factors reveal the internal structures of condensed electron pairs [34], and manifest themselves in optical response only at frequencies deep inside the superconducting band gap $\omega \ll \omega_g = \Delta/\hbar$ [32]. Previous works focused on unraveling these coherence factors in electrical transport [32, 33], quasiparticle scattering [34, 35], and nuclear spin relaxation [36–38]. Our central goal in this paper is to reveal the fingerprints of the superconducting coherence factors in thermal photonics, which can also open new frontiers in manipulating radiative heat transfer in energy harvesting devices with superconducting components.

Model.—As shown in Fig. 1(a), we consider a spherical gyromagnetic YIG nanoparticle with radius r at temperature T_1 placed near a niobium slab at temperature T_b . We assume that the particle is small compared to its distance z from the slab $r < z$ and consider the point-dipole approximation for the YIG nanoparticle. Following the framework of fluctuational electrodynamics [41], we find the net power P_1 absorbed by the YIG nanoparticle is [42],

$$P_1 = 8 \int_0^\infty d\omega \hbar \omega k_0^2 (n_b - n_1) \text{Tr}\{\text{Im}[\bar{\bar{G}}_m(\vec{r}_1, \vec{r}_1)] \text{Im}[\bar{\alpha}_1]\}, \quad (2)$$

where $k_0 = \omega/c$ is the vacuum wavenumber, $n_i = 1/(e^{\hbar\omega/k_B T_i} - 1)$ is the mean photon number at temperature T_i ($i = 1, b$), $\bar{\bar{G}}_m(\vec{r}_1, \vec{r}_1)$ is the near-field magnetic dyadic Green's function at the nanoparticle position \vec{r}_1 , and $\bar{\alpha}_1$ is the magnetic polarizability tensor of the YIG nanoparticle. As shown in Fig. 1(b), YIG typically has magnon resonance at GHz frequencies ω_{YIG} much lower than the superconducting band gap [43]. This leads to a peak of $\text{Im}[\bar{\alpha}_1]$ and spectral heat transfer at $\omega_{\text{YIG}} \ll \omega_g$ [43]. Therefore, from Eq. (2), NFRHT in our system is governed by low-frequency spectrum components deep inside the superconducting band gap, allowing the isolation of superconducting coherence effects in this ferromagnet-superconductor system. This is in stark contrast to NFRHT in previous metal/dielectric-superconductor systems, which is generally determined by spectrum components larger than or comparable to the superconducting band gap [25–27]. We further note that plasmon resonance in conventional metals or dielectrics is typically at frequencies much higher than the superconducting band gap and cannot be exploited to isolate superconducting coherence effects in thermal photonics (see Fig. 1(b)).

From Eq. (2), effects of Cooper pairs and Bogoliubov quasiparticles on NFRHT are encoded in the near-field magnetic Green's function $\bar{\bar{G}}_m$. Here, $\bar{\bar{G}}_m$ is dominated

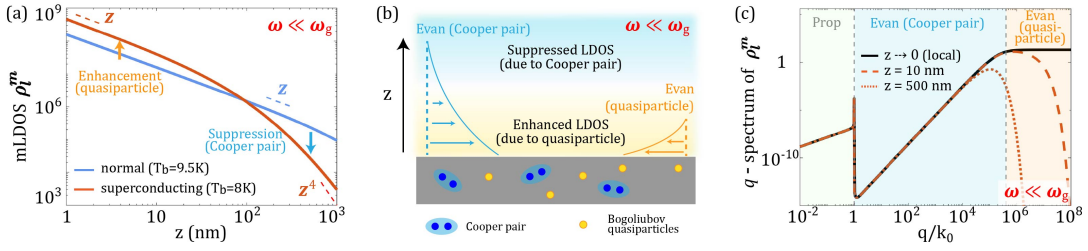


FIG. 2. Oposing effects of Cooper pairs and Bogoliubov quasiparticles on low-frequency near-field thermal radiation. (a) Dependence of low-frequency magnetic LDOS ρ_l^m on distance z from the niobium slab. In the superconducting phase, ρ_l^m is enhanced by Bogoliubov quasiparticle coherence at small distance, while suppressed by Cooper pairs screening effects at larger distance. (b) Sketch of evanescent waves associated with Bogoliubov quasiparticles and Cooper pairs. (c) Momentum q -spectrum of mLDOS ρ_l^m near a superconducting niobium slab at $T = 8$ K. High-momentum evanescent waves are dominated by Bogoliubov quasiparticles, while low-momentum evanescent waves are dominated by Cooper pair screening effects. We consider frequency $\omega = 2\pi$ GHz $\ll \omega_g = \Delta/\hbar \approx 2$ THz in this figure.

by evanescent waves and can be approximated as,

$$\bar{G}_m(\vec{r}_1, \vec{r}_1) \approx \frac{i}{8\pi^2 k_0^2} \int \frac{q dq}{k_z} e^{-2qz} r_s(q) \begin{bmatrix} -k_z^2 & 0 & 0 \\ 0 & -k_z^2 & 0 \\ 0 & 0 & 2q^2 \end{bmatrix}, \quad (3)$$

where $k_z = \sqrt{k_0^2 - q^2}$, q is the in-plane wavevector of evanescent waves, and z is the distance between \vec{r}_1 and the slab interface. The fresnel reflection coefficient $r_s(q)$ is determined by the permittivity of the niobium slab ϵ_{Nb} . In this paper, we consider the Drude model for ϵ_{Nb} in the normal phase, and Mattis-Bardeen theory [44, 45] for ϵ_{Nb} in the superconducting phase (see details in [42]). In the superconducting phase, Bogoliubov quasiparticles contribute to the dissipation of the superconductor, i.e., $\text{Im} \epsilon_{Nb}$. Different from normal conduction electrons, coherence factors of Bogoliubov quasiparticles introduce an additional factor,

$$u_{\mathbf{k}} u_{\mathbf{k}'} + v_{\mathbf{k}} v_{\mathbf{k}'}, \quad (4)$$

that renormalizes the scattering of a quasiparticle from a state \mathbf{k} to another state \mathbf{k}' upon absorption of a photon with momentum $\mathbf{k}' - \mathbf{k}$ [30, 31]. At low frequencies, this additional factor becomes prominent and leads to increased dissipation in the superconducting phase [32]. In contrast, Cooper pairs contribute to the screening effects (negative $\text{Re} \epsilon_{Nb}$) much stronger compared to the screening effects in the normal phase.

Near-field magnetic LDOS.—Our first goal is to isolate different effects of Cooper pairs and Bogoliubov quasiparticles on low-frequency near-field thermal radiation, which can be characterized by photonic local density of states (LDOS). In Fig. 2(a), we study low-frequency magnetic LDOS (mLDOS) $\rho_l^m = \omega \text{Tr}\{\text{Im}[\bar{G}_m(\vec{r}_1, \vec{r}_1)]\}/\pi c^2$ at 1 GHz near a superconducting niobium slab (transition temperature $T_c = 9.2$ K). We find that, right below the transition temperature T_c , low-frequency ρ_m is enhanced by around 3 times at small distance ($z < 100$ nm) from the superconducting slab, but is strongly suppressed at relatively larger distance ($z \geq 100$ nm).

As sketched in Fig. 2(b), the different behaviors of ρ_l^m in the small and large z regions at the superconducting phase transition originate from evanescent waves associated with different mechanisms. To elucidate this idea, we analyze the momentum q -spectrum of near-field mLDOS $\partial \rho_l^m / \partial q$ when the niobium slab is in the superconducting phase. As shown in Fig. 2(c), the q -spectrum can be divided into three regions corresponding to different mechanisms. At $q < k_0$, $k_z = \sqrt{k_0^2 - q^2}$ is real, indicating contributions from propagating waves. Meanwhile, at $q > k_0$, e^{-2qz} in Eq. (3) provides a momentum cut-off at $q \sim 1/2z$. Therefore, in the small z region, mLDOS ρ_l^m is dominated by contributions from high-momentum evanescent waves with $q \gg k_0$. In this region, we have,

$$\partial \rho_l^m / \partial q \approx \frac{\omega}{8\pi^2 c^2} \text{Im}[\epsilon_{Nb} - 1] e^{-2qz}. \quad (5)$$

We thus ascribe these high-momentum evanescent waves to dissipation associated with Bogoliubov quasiparticles. In this small z region, quantum coherence of Bogoliubov quasiparticles enhances the mLDOS ρ_l^m at the superconducting phase transition. Integrating Eq. (5) with respect to q , we find $\rho_l^m \sim z^{-1}$ matching our numeric calculations in Fig. 2(a).

At relatively larger z , magnetic LDOS ρ_l^m is dominated by contributions from evanescent waves with lower momentum. In this region, we have,

$$\partial \rho_l^m / \partial q \approx \frac{cq^3}{\pi^2 \omega^2} \text{Im}\left[\frac{i}{\sqrt{\epsilon_{Nb}}}\right] e^{-2qz}. \quad (6)$$

In the superconducting phase, $|\text{Re}[\epsilon_{Nb}]| \gg \text{Im}[\epsilon_{Nb}]$ at low frequencies. Therefore, we attribute these lower-momentum evanescent waves to be dominated by Cooper pairs. In this large z region, Cooper pair screening effects strongly suppress ρ_l^m at the superconducting phase transition. Integrating Eq. (6), we find the mLDOS $\rho_l^m \sim z^{-4}$ matching our numeric calculations in Fig. 2(a).

Superconducting coherence peak in NFRHT.—We now reveal the signatures of Bogoliubov quasiparticle coher-

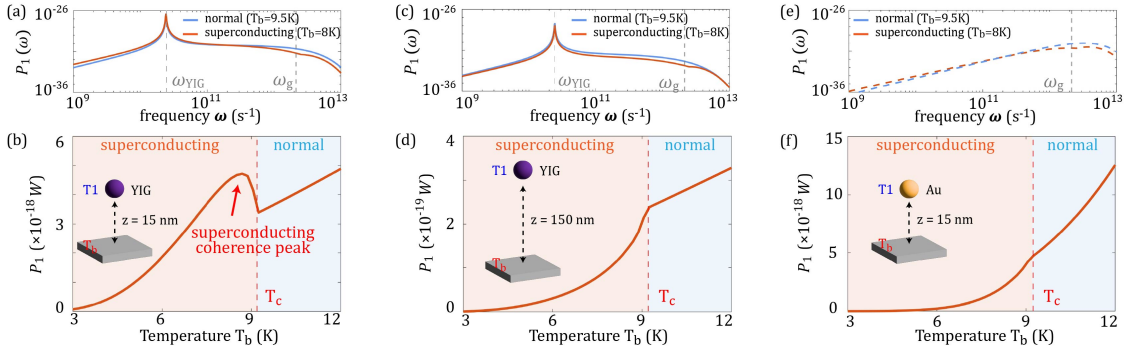


FIG. 3. Superconducting coherence peak in NFRHT due to Bogoliubov quasiparticle coherence. (a-d) Radiative heat transfer P_1 and spectral heat transfer $P_1(\omega)$ between a YIG nanoparticle and a niobium slab separated by (a,b) $z = 15$ nm or (c,d) $z = 150$ nm. (e,f) P_1 and $P_1(\omega)$ between a gold nanoparticle and a niobium slab separated by $z = 15$ nm. Quantum coherence of Bogoliubov quasiparticles leads to the peak of P_1 right below the transition temperature in (b). We consider $r = 6$ nm and $T_1 = 1$ K in this figure. Detailed material parameters are provided in Ref. [42].

ence in NFRHT. Evanescent waves associated with Bogoliubov quasiparticles and Cooper pairs lead to distinct NFRHT behaviors in the small and large z regions at the superconducting phase transition. We now consider NFRHT P_1 between a YIG nanoparticle at temperature $T_1 = 1$ K and a niobium slab at temperature T_b separated by $z = 15$ nm (Figs. 3(a,b)) and $z = 150$ nm (Figs. 3(c,d)). As shown in Figs. 3(a,c), YIG magnon resonance leads to a peak in spectral heat transfer $P_1(\omega)$ at ω_{YIG} . Therefore, NFRHT in this superconductor-ferromagnet system is dominated by low-frequency spectrum components at $\omega \ll \omega_g$.

For a small vacuum gap $z = 15$ nm, NFRHT is dominated by evanescent waves associated with Bogoliubov quasiparticles in the superconducting phase. Therefore, as shown in Fig. 3(b), we find that the heat transfer P_1 is enhanced right below the transition temperature T_c due to the quantum coherence of Bogoliubov quasiparticles. This reveals a superconducting ‘coherence peak’ in near-field thermal conductance, which is the fingerprint of superconductor coherence factors in thermal photonics. This peak leads to an unconventional negative temperature dependence of heat transfer P_1 at the superconducting phase transition, which is in stark contrast to the positive temperature dependence of blackbody radiation ($\propto T^3$) or radiation from conventional materials. Meanwhile, we find that P_1 decays fast at lower temperatures due to a reduced number of thermally excited Bogoliubov quasiparticles. We note the above NFRHT behaviors in this superconductor-ferromagnet system are in stark contrast to previous NFRHT observed in superconductor-normal-metal systems [25, 26] (also see Fig. 3(f)).

In contrast, for a relatively larger vacuum gap $z = 150$ nm, we find the heat transfer P_1 is strongly suppressed below the transition temperature T_c . This strong suppression originates from near-field thermal radiation dominated by Cooper pair screening effects. We note that, in this case, P_1 decreases monotonically with de-

creasing temperature, and the effects of superconducting coherence factors cannot be observed.

For comparison, in Figs. 3(e,f), we also demonstrate NFRHT between a gold nanoparticle and a niobium slab separated by $z = 15$ nm. As shown in Fig. 3(e), in stark contrast to YIG nanoparticles, NFRHT in this superconductor-normal-metal system is dominated by spectral components at frequencies $\omega \gtrsim \omega_g$. As shown in Fig. 3(f), P_1 decreases monotonically with decreasing temperature, and no superconducting ‘coherence peak’ is revealed in NFRHT.

Superconductivity effects on many-body NFRHT.—We have isolated the effects of Cooper pairs and Bogoliubov quasiparticles on magnetic LDOS and NFRHT between two bodies. Meanwhile, another important property of the near-field thermal radiation is its spatial coherence [23, 46], which is crucial for many-body NFRHT [41, 47]. As shown in Fig. 4(a), we now consider a 3×3 array of identical YIG nanoparticles with polarizability tensor $\bar{\alpha}_1$ at temperature T_1 near a niobium slab at temperature T_b . We consider all particles are maintained at the same temperature T_1 , thus there is no net heat transfer between the particles. We focus on the net thermal power P_{mb} absorbed by the central particle at position \vec{r}_1 in the array. Following the framework of fluctuational electrodynamics [41], we find,

$$P_{mb} = 8 \int_0^\infty d\omega \hbar \omega k_0^2 (n_b - n_1) \text{Im} \left\{ \sum_{jj'}^{N=9} \text{Tr} [[\bar{T}^{-1}]_{1j} [\bar{A}]_{jj} \text{Im} [\bar{G}]_{jj'} [\bar{A}^\dagger]_{j'j'} [\bar{T}^{-1}]_{j'1} [\bar{B}^\dagger]_{11}] \right\}, \quad (7)$$

where $\bar{T}_{ij} = \delta_{ij} \bar{I} - 4\pi k_0^2 (1 - \delta_{ij}) \bar{\alpha}_1 \bar{G}_{ij}$, $\bar{A}_{ij} = \delta_{ij} \bar{\alpha}_1$, $\bar{B}_{ij} = \delta_{ij} (\bar{\alpha}_1^{-1} + 4\pi k_0^2 \bar{G}_{ij})$, and $\bar{G}_{ij} = \bar{G}(\vec{r}_i, \vec{r}_j)$. \bar{I} is the 3×3 identity matrix and δ_{ij} is the Kronecker delta. We characterize the many-body effects on NFRHT by $\Delta P = P_{mb} - P_1$, which represent the differences of net power absorbed by the YIG nanoparticle with and without the

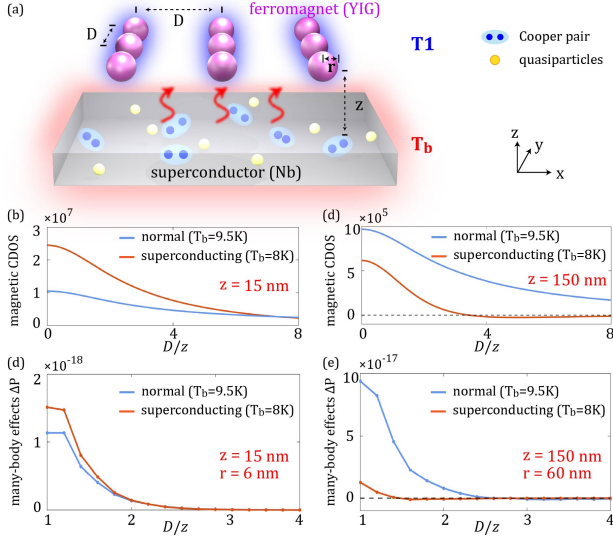


FIG. 4. Isolating effects of Cooper pairs and Bogoliubov quasiparticles on many-body NFRHT. (a) Schematic of NFRHT between a 3×3 YIG nanoparticle array at temperature T_1 and a niobium slab at temperature T_b . Nanoparticles are separated from the niobium slab by a distance z . (b,c) Magnetic cross density of states ρ_c^m at $\omega = 2\pi\text{GHz}$ at two points separated distance D at the same distance z from the niobium slab. (d,e) Many-body effects $\Delta P = P_{mb} - P_1$ on NFRHT when the niobium slab is in the normal phase or superconducting phase. Parameters are (d) $T_1 = 1\text{ K}$, $r = 6\text{ nm}$, $P_1(9.5\text{ K}) \approx 3.5 \times 10^{-18}\text{ W}$, $P_1(8\text{ K}) \approx 4.3 \times 10^{-18}\text{ W}$, and (e) $T_1 = 1\text{ K}$, $r = 60\text{ nm}$, $P_1(9.5\text{ K}) \approx 2.5 \times 10^{-16}\text{ W}$, $P_1(8\text{ K}) \approx 1.1 \times 10^{-16}\text{ W}$.

presence of other nanoparticles.

From Eq. (7), we note that many-body effects ΔP are largely determined by the spatial coherence of near-field thermal fluctuations proportional to $\text{Im}[\bar{G}(\vec{r}_j, \vec{r}_{j'})]$. Therefore, in Figs. 4(b,d), we first study the effects of superconductivity on the magnetic cross density of states (mCDOS) $\rho_c^m = \omega \text{Tr}\{\text{Im}[\bar{G}_m(\vec{r}_1, \vec{r}_2)]\}/\pi c^2$, which characterize the correlations of thermal fluctuations at two points \vec{r}_1 and \vec{r}_2 . We focus on ρ_c^m at two points separated by distance $D = |\vec{r}_1 - \vec{r}_2|$ at the same distance z from the niobium slab. Similar to mLDOS, evanescent waves associated with Cooper pairs and Bogoliubov quasiparticles lead to distinct behaviors of mCDOS in the small and large z regions at the superconducting phase transition. As shown in Fig. 4(b), in the small $z = 15\text{ nm}$ region, we find that mCDOS at two points separated by small distance D are enhanced by quantum coherence of Bogoliubov quasiparticles. Meanwhile, at larger separation D , mCDOS are suppressed due to Cooper pair screening effects. In contrast, as shown in Fig. 4(d), we find mCDOS at large $z = 150\text{ nm}$ are strongly suppressed at all D due to Cooper pair screening effects. In general, we find that Cooper pair screening effects suppress the spatial coherence length of near-field thermal radiation.

The above mCDOS ρ_c^m behaviors lead to interesting

many-body radiative heat transfer effects ΔP at the superconducting phase transition. In Figs. 4(c,e), we consider a YIG nanoparticle array with lattice constant D in the small $z = 15\text{ nm}$ and large $z = 150\text{ nm}$ regions. In general, NFRHT is enhanced by many-body effects, i.e., $\Delta P > 0$. Meanwhile, as shown in Fig. 4(c), we find that coherence of Bogoliubov quasiparticles enhances many-body effects ΔP right below the transition temperature in the small z region. In contrast, as shown in Fig. 4(e), Cooper pair screening effects suppress the many-body effects ΔP in the superconducting phase. In addition, we note that, for NFRHT in extended nanoparticle arrays (large D) in the large z region, Cooper pair screening effects can turn many-body effects from enhancement ($\Delta P > 0$) to suppression ($\Delta P < 0$). The above analysis isolates the different effects of Bogoliubov quasiparticles and Cooper pairs on many-body NFRHT.

Discussions.—In summary, we reveal a superconducting coherence peak in NFRHT in the superconductor-ferromagnet system and isolate effects of Cooper pairs and Bogoliubov quasiparticles on NFRHT. Our predicted phenomenon can be experimentally observed in state-of-the-art experimental platforms, e.g., scanning thermal microscopy (SThM) probes [48, 49], which can probe nanoscale radiative heat transfer across a vacuum gap $\lesssim 10\text{ nm}$. Our results are important for developing nanoscale energy harvesting technologies, e.g., thermal diodes or rectifiers [50, 51], in superconducting circuits.

Beyond this, our discussions of low-frequency magnetic LDOS and CDOS are also important for quantum dynamics of spin qubits near superconductors, e.g., spin dephasing [52] and relaxation [53, 54].

Acknowledgments.—W.S. and Z.J. acknowledge support from the U.S. Department of Energy (DOE), Office of Basic Sciences under DE-SC0017717 and the Army Research Office under grant number W911NF-21-1-0287. Z.M.Z. acknowledges support from the U.S. Department of Energy (DOE), Office of Science, Basic Energy Sciences under Grant No. DE-SC0018369.

* zjacob@purdue.edu

- [1] S.-A. Biehs, R. Messina, P. S. Venkataram, A. W. Rodriguez, J. C. Cuevas, and P. Ben-Abdallah, *Reviews of Modern Physics* **93**, 025009 (2021).
- [2] A. Volokitin and B. N. Persson, *Reviews of Modern Physics* **79**, 1291 (2007).
- [3] Z. M. Zhang, *Nano/microscale heat transfer*, 2nd ed. (Springer Cham, 2020).
- [4] H. Salihoglu, J. Shi, Z. Li, Z. Wang, X. Luo, I. Bondarev, S.-A. Biehs, and S. Shen, *Physical Review Letters* **131**, 086901 (2023).
- [5] A. Volokitin and B. Persson, *Physical Review B* **65**, 115419 (2002).
- [6] S. A. Hassani Gangaraj and F. Monticone, *ACS photonics* **9**, 806 (2022).

- [7] O. Ilic, N. H. Thomas, T. Christensen, M. C. Sherrott, M. Soljagic, A. J. Minnich, O. D. Miller, and H. A. Atwater, *ACS nano* **12**, 2474 (2018).
- [8] T. Tokunaga, A. Jarzembki, T. Shiga, K. Park, and M. Francoeur, *Physical Review B* **104**, 125404 (2021).
- [9] Y. Tan, B. Liu, S. Shen, and Z. Yu, *Nanophotonics* **5**, 22 (2016).
- [10] H. Kallel, R. Carminati, and K. Joulain, *Physical Review B* **95**, 115402 (2017).
- [11] D. Feng, X. Yang, Z. Han, and X. Ruan, *Physical Review B* **109**, L081409 (2024).
- [12] K. Sasihithlu and G. S. Agarwal, *Nanophotonics* **7**, 1581 (2018).
- [13] D. Feng, X. Yang, and X. Ruan, *Nano Letters* **23**, 10044 (2023).
- [14] Y. Guo, C. L. Cortes, S. Molesky, and Z. Jacob, *Applied Physics Letters* **101** (2012).
- [15] D. Feng, X. Ruan, S. K. Yee, and Z. M. Zhang, *Nano Energy* **103**, 107831 (2022).
- [16] P. S. Venkataram, S. Molesky, W. Jin, and A. W. Rodriguez, *Physical Review Letters* **124**, 013904 (2020).
- [17] B. Zhao, B. Guizal, Z. M. Zhang, S. Fan, and M. Antezza, *Physical Review B* **95**, 245437 (2017).
- [18] M. Luo, Y. Jeyar, B. Guizal, and M. Antezza, *Physical Review B* **110**, 075423 (2024).
- [19] K. Asheichyk and M. Krüger, *Physical Review B* **109**, 125412 (2024).
- [20] J. R. Nolen, A. C. Overvig, M. Cotrufo, and A. Alù, *Nature Nanotechnology* , 1 (2024).
- [21] X. Huang, C. Yeung, and A. P. Raman, *Physical Review Applied* **19**, 034037 (2023).
- [22] J.-J. Greffet and C. Henkel, *Contemporary Physics* **48**, 183 (2007).
- [23] R. Yu and S. Fan, *Physical Review Letters* **130**, 096902 (2023).
- [24] C.-L. Zhou, Z. Torbatian, S.-H. Yang, Y. Zhang, H.-L. Yi, M. Antezza, D. Novko, and C.-W. Qiu, *Physical Review Letters* **133**, 066902 (2024).
- [25] T. Králík, V. Musilová, T. Fořt, and A. Srnka, *Physical Review B* **95**, 060503 (2017).
- [26] V. Musilová, T. Králík, T. Fořt, and M. Macek, *Physical Review B* **99**, 024511 (2019).
- [27] E. Moncada-Villa and J. Cuevas, *Physical Review Applied* **15**, 024036 (2021).
- [28] S. Castillo-López, C. Villarreal, R. Esquivel-Sirvent, and G. Pirruccio, *International Journal of Heat and Mass Transfer* **182**, 121922 (2022).
- [29] W. DeGottardi, M. J. Gullans, S. Hegde, S. Vishveshvara, and M. Hafezi, *Physical Review B* **99**, 235124 (2019).
- [30] M. Dressel, *Advances in Condensed Matter Physics* **2013**, 104379 (2013).
- [31] P. Coleman, *Introduction to many-body physics* (Cambridge University Press, 2015).
- [32] O. Klein, E. Nicol, K. Holczer, and G. Grüner, *Physical Review B* **50**, 6307 (1994).
- [33] R. Boyack, S. Mirabi, and F. Marsiglio, *Communications Physics* **6**, 54 (2023).
- [34] T. Hanaguri, Y. Kohsaka, M. Ono, M. Maltseva, P. Coleman, I. Yamada, M. Azuma, M. Takano, K. Ohishi, and H. Takagi, *Science* **323**, 923 (2009).
- [35] C. Zou, Z. Hao, X. Luo, S. Ye, Q. Gao, M. Xu, X. Li, P. Cai, C. Lin, X. Zhou, *et al.*, *Nature Physics* **18**, 551 (2022).
- [36] L. Hebel and C. P. Slichter, *Physical Review* **113**, 1504 (1959).
- [37] Y. Dai, A. Kreisel, and B. M. Andersen, *Physical Review B* **110**, 144516 (2024).
- [38] Z. Li, C. Mu, P. Li, W. Wu, J. Hu, T. Xiang, K. Jiang, and J. Luo, *Physical Review X* **14**, 041072 (2024).
- [39] J. Campuzano, H. Ding, M. Norman, M. Randeira, A. Bellman, T. Yokoya, T. Takahashi, H. Katayama-Yoshida, T. Mochiku, and K. Kadowaki, *Physical review B* **53**, R14737 (1996).
- [40] K. Fujita, I. Grigorenko, J. Lee, W. Wang, J. X. Zhu, J. Davis, H. Eisaki, S.-i. Uchida, and A. V. Balatsky, *Physical Review B* **78**, 054510 (2008).
- [41] R. Messina, M. Tschikin, S.-A. Biehs, and P. Ben-Abdallah, *Physical Review B—Condensed Matter and Materials Physics* **88**, 104307 (2013).
- [42] See Supplementary Material for derivations and additional calculation details, which include Refs. [55–62].
- [43] F. Khosravi, W. Sun, C. Khandekar, T. Li, and Z. Jacob, *New Journal of Physics* **26**, 053006 (2024).
- [44] D. C. Mattis and J. Bardeen, *Physical Review* **111**, 412 (1958).
- [45] R. Pöpel, *Journal of applied physics* **66**, 5950 (1989).
- [46] E. Bailly, J.-P. Hugonin, B. Vest, and J.-J. Greffet, *Physical Review Research* **3**, L032040 (2021).
- [47] L. Zhu, Y. Guo, and S. Fan, *Physical Review B* **97**, 094302 (2018).
- [48] K. Kim, B. Song, V. Fernández-Hurtado, W. Lee, W. Jeong, L. Cui, D. Thompson, J. Feist, M. H. Reid, F. J. García-Vidal, *et al.*, *Nature* **528**, 387 (2015).
- [49] L. Cui, W. Jeong, V. Fernández-Hurtado, J. Feist, F. J. García-Vidal, J. C. Cuevas, E. Meyhofer, and P. Reddy, *Nature communications* **8**, 14479 (2017).
- [50] S. O. Kasali, J. Ordonez-Miranda, and K. Joulain, *International Journal of Heat and Mass Transfer* **154**, 119739 (2020).
- [51] P. Ben-Abdallah and S.-A. Biehs, *Applied Physics Letters* **103** (2013).
- [52] W. Sun, A. E. R. López, and Z. Jacob, *arXiv preprint arXiv:2402.18816* (2024).
- [53] S. P. Kelly and Y. Tserkovnyak, *arXiv preprint arXiv:2412.05465* (2024).
- [54] S. Li, S. P. Kelly, J. Zhou, H. Lu, Y. Tserkovnyak, H. Wang, and C. R. Du, *arXiv preprint arXiv:2412.18896* (2024).
- [55] B. D. Cullity and C. D. Graham, *Introduction to magnetic materials* (John Wiley & Sons, 2011).
- [56] R. D. Sanchez, J. Rivas, P. Vaqueiro, M. Lopez-Quintela, and D. Caeiro, *Journal of magnetism and magnetic materials* **247**, 92 (2002).
- [57] M. Rajendran, S. Deka, P. Joy, and A. Bhattacharya, *Journal of Magnetism and Magnetic Materials* **301**, 212 (2006).
- [58] A. H. Sihvola, *Optics letters* **19**, 430 (1994).
- [59] A. V. Pronin, M. Dressel, A. Pimenov, A. Loidl, I. V. Roshchin, and L. Greene, *Physical Review B* **57**, 14416 (1998).
- [60] A. Gubin, K. Il'in, S. Vitusevich, M. Siegel, and N. Klein, *Physical Review B* **72**, 064503 (2005).
- [61] L. Mattheiss, *Physical Review B* **1**, 373 (1970).
- [62] L. Novotny and B. Hecht, *Principles of nano-optics* (Cambridge university press, 2012).

Supplementary Material for ‘Superconducting coherence peak in near-field radiative heat transfer’

Wenbo Sun,¹ Zhuomin M. Zhang,² and Zubin Jacob^{1,*}

¹*Elmore Family School of Electrical and Computer Engineering,
Birck Nanotechnology Center, Purdue University, West Lafayette, Indiana 47907, USA*

²*George W. Woodruff School of Mechanical Engineering,
Georgia Institute of Technology, Atlanta, Georgia 30332, USA*

(Dated: March 11, 2025)

S1. MANY-BODY RADIATIVE HEAT TRANSFER THEORY

In this appendix, we provide detailed derivations of the many-body near-field radiative heat transfer (NFRHT) between ferromagnetic yttrium iron garnet (YIG) nanoparticles and the superconductor slab. Our derivations follow the many-body radiative heat transfer theory based on fluctuational electrodynamics [1, 2].

We consider an ensemble of N YIG nanoparticles placed near a superconducting niobium slab. Superconductivity effects from the niobium slab are encoded in the near-field magnetic Green’s function $\bar{\bar{G}}_m$. In the following derivation, we suppress the subscript m to simplify the notation and only write $\bar{\bar{G}}$. We consider small nanoparticle sizes and employ the point dipole approximation for YIG nanoparticles. The net power P_i absorbed by the i th nanoparticle is,

$$P_i = \langle \frac{d\vec{m}_i}{dt} \cdot \vec{H}_i(t) \rangle = 2 \int_0^\infty \frac{d\omega}{2\pi} \omega \int_0^\infty \frac{d\omega'}{2\pi} \text{Im} \left[\langle \vec{m}_i(\omega) \cdot \vec{H}_i^\dagger(\omega') \rangle e^{-i(\omega-\omega')t} \right], \quad (\text{S1})$$

where \vec{m}_i is the magnetic dipole moment of the i th nanoparticle, \vec{H}_i^\dagger is the Hermitian conjugate of \vec{H}_i , and \vec{H}_i is the magnetic field at the position of the i th nanoparticle. \vec{m}_i and \vec{H}_i can be further decomposed into the fluctuating and induced components,

$$\vec{m}_i = \vec{m}_i^{fl} + \vec{m}_i^{ind}, \quad \vec{H}_i = \vec{H}_i^{fl} + \vec{H}_i^{ind}, \quad (\text{S2})$$

where \vec{m}_i^{ind} is the magnetic dipole moment induced by fluctuating fields \vec{H}_i^{fl} , and \vec{H}_i^{ind} is the magnetic field induced by fluctuating dipole moment \vec{m}_i^{fl} . We have,

$$\vec{H}_i = \vec{H}_i^{fl} + 4\pi k_0^2 \sum_j \bar{\bar{G}}_{ij} \vec{m}_j, \quad (\text{S3})$$

$$\vec{m}_i = \vec{m}_i^{fl} + \bar{\bar{\alpha}}_i (\vec{H}_i^{fl} + 4\pi k_0^2 \sum_{j \neq i} \bar{\bar{G}}_{ij} \vec{m}_j), \quad (\text{S4})$$

where $\bar{\bar{G}}_{ij} = \bar{\bar{G}}(\vec{r}_i, \vec{r}_j, \omega)$ and $\bar{\bar{\alpha}}_i$ is the polarizability tensor of the i th YIG nanoparticle. From Eqs. (S3,S4), we can find that

$$\begin{bmatrix} \vec{m}_1 \\ \vdots \\ \vec{m}_N \end{bmatrix} = \bar{\bar{T}}^{-1} \begin{bmatrix} \vec{m}_1^{fl} \\ \vdots \\ \vec{m}_N^{fl} \end{bmatrix} + \bar{\bar{T}}^{-1} \bar{\bar{A}} \begin{bmatrix} \vec{H}_1^{fl} \\ \vdots \\ \vec{H}_N^{fl} \end{bmatrix} = \bar{\bar{M}} \begin{bmatrix} \vec{m}_1^{fl} \\ \vdots \\ \vec{m}_N^{fl} \end{bmatrix} + \bar{\bar{N}} \begin{bmatrix} \vec{H}_1^{fl} \\ \vdots \\ \vec{H}_N^{fl} \end{bmatrix}, \quad (\text{S5})$$

$$\begin{bmatrix} \vec{H}_1 \\ \vdots \\ \vec{H}_N \end{bmatrix} = \bar{\bar{D}} \bar{\bar{T}}^{-1} \begin{bmatrix} \vec{m}_1^{fl} \\ \vdots \\ \vec{m}_N^{fl} \end{bmatrix} + (\bar{\bar{I}}_{3N} + \bar{\bar{D}} \bar{\bar{T}}^{-1} \bar{\bar{A}}) \begin{bmatrix} \vec{H}_1^{fl} \\ \vdots \\ \vec{H}_N^{fl} \end{bmatrix} = \bar{\bar{O}} \begin{bmatrix} \vec{m}_1^{fl} \\ \vdots \\ \vec{m}_N^{fl} \end{bmatrix} + \bar{\bar{P}} \begin{bmatrix} \vec{H}_1^{fl} \\ \vdots \\ \vec{H}_N^{fl} \end{bmatrix}, \quad (\text{S6})$$

where $\bar{\bar{I}}_{3N}$ is the $3N \times 3N$ identity matrix. $\bar{\bar{T}}, \bar{\bar{A}}, \bar{\bar{D}}$ are $N \times N$ block matrices with each element being a 3×3 matrix,

$$\bar{\bar{T}}_{ij} = \delta_{ij} \bar{\bar{I}}_3 - 4\pi k_0^2 (1 - \delta_{ij}) \bar{\bar{\alpha}}_i \bar{\bar{G}}_{ij}, \quad \bar{\bar{A}}_{ij} = \delta_{ij} \bar{\bar{\alpha}}_i, \quad \bar{\bar{D}}_{ij} = 4\pi k_0^2 \bar{\bar{G}}_{ij}, \quad (\text{S7})$$

* zjacob@purdue.edu

where \bar{I}_3 is the 3×3 identity matrix. Following Refs. [2], we also define $\bar{B} = \bar{D} + \bar{A}^{-1}\bar{T}$. \bar{B} is also a $N \times N$ block matrix with element

$$\bar{B}_{ij} = \delta_{ij}[\bar{\alpha}_i^{-1} + \bar{D}_{ij}]. \quad (\text{S8})$$

Substituting Eqs. (S5-S6) into Eq. (S1), we find,

$$\langle \bar{m}_i(\omega) \cdot \bar{H}_i^\dagger(\omega') \rangle = \sum_{\alpha} \sum_{\beta\beta'} \sum_{jj'} \left([\bar{M}_{ij}]_{\alpha\beta} \langle [\bar{m}_j^{fl}]_{\beta} [\bar{m}_{j'}^{fl\dagger}]_{\beta'} \rangle [\bar{O}_{j'i}^\dagger]_{\beta'\alpha} + [\bar{N}_{ij}]_{\alpha\beta} \langle [\bar{H}_j^{fl}]_{\beta} [\bar{H}_{j'}^{fl\dagger}]_{\beta'} \rangle [\bar{P}_{j'i}^\dagger]_{\beta'\alpha} \right), \quad (\text{S9})$$

where $[\bar{M}_{ij}]_{\alpha\beta}$ denotes the element of the 3×3 matrix \bar{M}_{ij} and $[\bar{m}_j^{fl}]_{\beta}$ denotes the element of the 3×1 vector \bar{m}_j^{fl} . In the above derivation, we use $\langle [\bar{m}_j^{fl}]_{\beta} [\bar{H}_{j'}^{fl\dagger}]_{\beta'} \rangle = 0$, i.e., there is no correlation between the magnetic dipole fluctuations and magnetic field fluctuations, to simplify the expression. The fluctuations $\langle [\bar{m}_j^{fl}]_{\beta} [\bar{m}_{j'}^{fl\dagger}]_{\beta'} \rangle$ and $\langle [\bar{H}_j^{fl}]_{\beta} [\bar{H}_{j'}^{fl\dagger}]_{\beta'} \rangle$ can be evaluated using the fluctuation-dissipation theorem,

$$\langle [\bar{m}_j^{fl}]_{\beta} [\bar{m}_{j'}^{fl\dagger}]_{\beta'} \rangle = 4\pi\hbar\delta(\omega - \omega')\delta_{jj'}(n_j + \frac{1}{2}) \left(\frac{\bar{\alpha}_j - \bar{\alpha}_j^\dagger}{2i} \right)_{\beta\beta'}, \quad (\text{S10})$$

$$\langle [\bar{H}_j^{fl}]_{\beta} [\bar{H}_{j'}^{fl\dagger}]_{\beta'} \rangle = 4\pi k_0^2 4\pi\hbar\delta(\omega - \omega')(n_b + \frac{1}{2}) \left(\frac{[\bar{G}]_{jj'} - [\bar{G}]_{j'j}^\dagger}{2i} \right)_{\beta\beta'}, \quad (\text{S11})$$

where n_i and n_b are the mean photon number at the i th particle temperature T_i and environment temperature T_b ,

$$n_i = \frac{1}{e^{\hbar\omega/k_B T_i} - 1}, \quad n_b = \frac{1}{e^{\hbar\omega/k_B T_b} - 1}. \quad (\text{S12})$$

Substituting Eqs. (S10,S11) into Eq. (S9), we obtain,

$$\langle \bar{m}_i(\omega) \cdot \bar{H}_i^\dagger(\omega') \rangle = 4\pi\hbar\delta(\omega - \omega') \left\{ \sum_j (n_j + \frac{1}{2}) \text{Tr}[\bar{M}_{ij} \bar{\chi}_{jj} \bar{O}_{ji}^\dagger] + 4\pi k_0^2 (n_b + \frac{1}{2}) \sum_{jj'} \text{Tr}[\bar{N}_{ij} \text{Im}[\bar{G}_{jj'}] \bar{P}_{j'i}^\dagger] \right\}, \quad (\text{S13})$$

where $\bar{\chi}_{jj} = (\bar{\alpha}_j - \bar{\alpha}_j^\dagger)/2i$. Since the photonic environment near BCS superconductor is reciprocal, we also have $([\bar{G}]_{jj'} - [\bar{G}]_{j'j}^\dagger)/2i = \text{Im}[\bar{G}_{j'j}]$.

In the main text, we consider all particles to have the same temperature. Substitute Eqs. (S7-S8) into Eq. (S13) and simplify Eq. (S13) by using the second law of thermodynamics, we find,

$$P_i = 8k_0^2 \int_0^\infty d\omega \hbar\omega (n_b - n_i) \text{Im} \left\{ \sum_{jj'}^N \text{Tr}[\bar{T}^{-1}]_{ij} [\bar{A}]_{jj} \text{Im}[\bar{G}]_{jj'} [\bar{A}^\dagger]_{j'j'} [\bar{T}^{-1,\dagger}]_{j'i} [\bar{B}^\dagger]_{ii} \right\}, \quad (\text{S14})$$

which is Eq. (7) in the main text. For the special case $N = 1$, we find Eq. (S14) is reduced to,

$$P_1 = 8k_0^2 \int_0^\infty d\omega \hbar\omega (n_b - n_1) \text{Tr}[\text{Im}[\bar{G}_{11}] \text{Im}[\bar{\alpha}_1]], \quad (\text{S15})$$

which is the net power absorbed by a single nanoparticle from the environment (Eq. (2) in the main text).

S2. ELECTROMAGNETIC RESPONSE OF BCS SUPERCONDUCTORS

In this Appendix, we provide the model and parameters for the permittivity ϵ_{Nb} of the niobium slab considered in the main text. Niobium typically has the superconducting phase transition temperature at $T_c = 9.2$ K. In the normal phase, we consider the Drude model for ϵ_{Nb} ,

$$\epsilon_{\text{Nb}} = 1 - \frac{\omega_p^2 \tau^2}{\omega^2 \tau^2 + 1} + i \frac{\sigma_n}{\epsilon_0 \omega (1 + \omega^2 \tau^2)}, \quad (\text{S16})$$

where we consider the normal state conductivity $\sigma_n = 2 \times 10^7$ S/m, plasma frequency $\omega_p = 8.8 \times 10^{15}$ Hz [3, 4], and corresponding electron relaxation time $\tau \approx 2.9 \times 10^{-14}$ s.

A. Mattis-Bardeen theory

In the superconducting phase, we consider the Mattis-Bardeen theory for niobium permittivity ε_{Nb} . Mattis-Bardeen theory is applicable to weak-coupling s-wave BCS superconductors with arbitrary purity and with local or nonlocal EM response, and matches well with experimental measurements [5].

The general form of nonlocal permittivity $\varepsilon_{\text{Nb}}(k, \omega)$ predicted by the Mattis-Bardeen theory is [6, 7],

$$\varepsilon_{\text{Nb}}(k, \omega) = 1 - \frac{3\sigma_n K_1(k, \omega)}{\hbar\varepsilon_0\omega^2} + i\frac{3\sigma_n K_2(k, \omega)}{\hbar\varepsilon_0\omega^2}, \quad (\text{S17a})$$

$$\begin{aligned} K_1(k, \omega) = \beta \left\{ \int_{\Delta}^{\infty} dE [f(E) - f(E + \hbar\omega)] [g_1(E) + 1] S(a_-, \beta) \right. \\ \left. - \int_{\Delta}^{\infty} dE [1 - f(E) - f(E + \hbar\omega)] [g_1(E) - 1] S(a_+, \beta) \right. \\ \left. + \int_{\max\{\Delta - \hbar\omega, -\Delta\}}^{\Delta} dE [1 - 2f(E + \hbar\omega)] \left\{ g_2(E) R(a_2, |a_1| + \beta) + S(a_2, |a_1| + \beta) \right\} \right. \\ \left. + \frac{\Theta(\hbar\omega - 2\Delta)}{2} \int_{\Delta - \hbar\omega}^{-\Delta} dE [1 - 2f(E + \hbar\omega)] \left\{ [g_1(E) + 1] S(a_-, \beta) - [g_1(E) - 1] S(a_+, \beta) \right\} \right\}, \quad (\text{S17b}) \end{aligned}$$

$$\begin{aligned} K_2(k, \omega) = \beta \left\{ \int_{\Delta}^{\infty} dE [f(E) - f(E + \hbar\omega)] \left\{ [g_1(E) + 1] R(a_-, \beta) + [g_1(E) - 1] R(a_+, \beta) \right\} \right. \\ \left. - \frac{\Theta(\hbar\omega - 2\Delta)}{2} \int_{\Delta - \hbar\omega}^{-\Delta} dE [1 - 2f(E + \hbar\omega)] \left\{ [g_1(E) + 1] R(a_-, \beta) + [g_1(E) - 1] R(a_+, \beta) \right\} \right\}, \quad (\text{S17c}) \end{aligned}$$

where

$$f(E) = 1/(1 + e^{E/k_b T}), \quad \beta = 1/kl, \quad (\text{S18a})$$

$$S(a, b) = \frac{a}{2} - \frac{ab}{2} \left[\arctan\left(\frac{2b}{b^2 + a^2 - 1}\right) + \Theta(1 - b^2 - a^2)\pi \right] + \frac{1}{8}(1 + b^2 - a^2) \ln\left(\frac{b^2 + (1 + a)^2}{b^2 + (1 - 1)^2}\right), \quad (\text{S18b})$$

$$R(a, b) = -\frac{b}{2} + \frac{ab}{4} \ln\left(\frac{b^2 + (1 + a)^2}{b^2 + (1 - 1)^2}\right) + \frac{1}{4}(1 + b^2 - a^2) \left[\arctan\left(\frac{2b}{b^2 + a^2 - 1}\right) + \Theta(1 - b^2 - a^2)\pi \right], \quad (\text{S18c})$$

$$g_1 = \frac{E^2 + \Delta^2 + \hbar\omega E}{\sqrt{E^2 - \Delta^2} \sqrt{(E + \hbar\omega)^2 - \Delta^2}}, \quad g_2 = \frac{E^2 + \Delta^2 + \hbar\omega E}{\sqrt{\Delta^2 - E^2} \sqrt{(E + \hbar\omega)^2 - \Delta^2}}, \quad (\text{S18d})$$

$$a_1 = \frac{\sqrt{E^2 - \Delta^2}}{\hbar v_F q}, \quad a_2 = \frac{\sqrt{(E + \hbar\omega)^2 - \Delta^2}}{\hbar v_F q}, \quad a_- = a_2 - a_1, \quad a_+ = a_1 + a_2, \quad (\text{S18e})$$

where Θ is the Heaviside step function, v_F is the Fermi velocity, and k_b is the Boltzmann constant. In the paper, we consider the Fermi velocity $v_F \approx 5 \times 10^5$ m/s for niobium [8]. In Eq. (S17), the screening effects $\text{Re } \varepsilon_{\text{Nb}}$ are dominated by the Cooper pair response, while dissipation $\text{Im } \varepsilon_{\text{Nb}}$ is dominated by the Bogoliubov quasiparticle response [9].

From Eq. (S17), we find at $k \gg 1/l$, nonlocal effects are not prominent, i.e., $\varepsilon_{\text{Nb}}(k, \omega) \approx \varepsilon_{\text{Nb}}(0, \omega)$. Therefore, in the main text, we consider the local limit $\varepsilon_{\text{Nb}}(k \rightarrow 0, \omega)$ in our calculations.

S3. MAGNETIC POLARIZABILITY TENSOR OF YIG AND GOLD NANOPARTICLES

In this Appendix, we provide the YIG permeability tensor $\bar{\mu}_{\text{YIG}}$ described by the Landau-Lifshitz-Gilbert equations [10]. We start from the free energy H of the spherical ferromagnetic YIG nanoparticle that contains the Zeeman energy and anisotropy energy,

$$H = -\mu_0 M_s \vec{\mathcal{M}} \cdot \vec{\mathbf{H}}_{\text{ext}} - K_x m_x^2, \quad (\text{S19})$$

where $\vec{\mathcal{M}}$ is the normalized magnetic direction vector, M_x is the x component of $\vec{\mathcal{M}}$, M_s is the saturation magnetization, and K_x is the anisotropy constant. In Eq. (S19), we consider the YIG nanoparticle to have uniaxial anisotropy with the anisotropy axis along the x -direction. From Eq. (S19), we find the effective field $\vec{\mathbf{H}}_{\text{eff}}$ is,

$$\vec{\mathbf{H}}_{\text{eff}} = -\frac{1}{\mu_0 M_s} \frac{\partial H}{\partial \vec{\mathcal{M}}} = \vec{\mathbf{H}}_{\text{ext}} + 2 \frac{K_{\parallel}}{\mu_0 M_s} m_x \hat{\mathbf{x}} = \vec{\mathbf{H}}_{\text{ext}} + H_k m_x \hat{\mathbf{x}}. \quad (\text{S20})$$

In this work, YIG nanoparticles are not subject to the external magnetic field, i.e., $\vec{\mathbf{H}}_{\text{ext}} = 0$. Therefore, the equilibrium magnetization is along the $\hat{\mathbf{x}}$ direction. Substitute Eq. (S20) in to the Landau-Lifshitz-Gilbert equation, we have,

$$\frac{d\vec{\mathcal{M}}}{dt} = -\mu_0 \gamma \vec{\mathcal{M}} \times \mathbf{H}_{\text{eff}} + \alpha_{\text{loss}} \vec{\mathcal{M}} \times \frac{d\vec{\mathcal{M}}}{dt}, \quad (\text{S21})$$

where α_{loss} is the Gilbert damping constant describing the loss of the ferromagnet and γ is the gyromagnetic ratio. The permeability tensor is then conventionally solved from Eq. (S21) by considering the perturbation of $\delta \vec{\mathcal{M}}$ under a small external magnetic field $\delta \vec{\mathbf{H}}$ [10]. We find the magnetic resonance frequency (in the absence of external magnetic fields) $\omega_r = \gamma \mu_0 H_k$, and the permeability tensor,

$$\bar{\mu}_{\text{YIG}} = \begin{bmatrix} 1 & 0 & 0 \\ 0 & 1 + \frac{\omega_m(\omega_r - i\alpha\omega)}{(\omega_r - i\alpha\omega)^2 - \omega^2} & -i \frac{\omega_m \omega}{(\omega_r - i\alpha\omega)^2 - \omega^2} \\ 0 & i \frac{\omega_m \omega}{(\omega_r - i\alpha\omega)^2 - \omega^2} & 1 + \frac{\omega_m(\omega_r - i\alpha\omega)}{(\omega_r - i\alpha\omega)^2 - \omega^2} \end{bmatrix}, \quad (\text{S22})$$

where $\omega_m = \gamma \mu_0 M_s$. In the main text, we consider $\alpha = 0.01$, $4\pi M_s = 1819$ G, and $H_k = 600$ G comparable to experimental values [11, 12]. The magnetic polarizability tensor for the gyromagnetic YIG nanoparticle can be obtained from $\bar{\mu}_{\text{YIG}}$ using the method in Ref. [13],

$$\bar{\alpha}_{\text{YIG}} = r^3 \begin{bmatrix} \frac{-1 + \mu_{xx}}{2 + \mu_{xx}} & 0 & 0 \\ 0 & \frac{(\mu_{yy} - 1)(\mu_{zz} + 2) + u_{yz}^2}{(\mu_{yy} + 2)(\mu_{zz} + 2) + u_{yz}^2} & \frac{3\mu_{yz}}{(\mu_{yy} + 2)(\mu_{zz} + 2) + u_{yz}^2} \\ 0 & -\frac{3\mu_{yz}}{(\mu_{yy} + 2)(\mu_{zz} + 2) + u_{yz}^2} & \frac{(\mu_{zz} - 1)(\mu_{yy} + 2) + u_{yz}^2}{(\mu_{yy} + 2)(\mu_{zz} + 2) + u_{yz}^2} \end{bmatrix}. \quad (\text{S23})$$

A. Polarizability tensor for gold nanoparticles

In the main text, we also consider NFRHT for gold nanoparticles to compare with ferromagnetic YIG nanoparticles. In this work, we consider the Drude model Eq. (S16) for gold permittivity ε_{au} . We consider the gold conductivity $\sigma_{\text{au}} = 5 \times 10^7$ S/m and the plasma frequency $\omega_p \approx 1.3 \times 10^{16}$ Hz.

In our calculations, we consider contributions from both magnetic and electric dipole moment fluctuations of the gold nanoparticle to NFRHT. The electric and magnetic polarizability of a gold nanoparticle with radius r is [14],

$$\alpha_{\text{au},e} = r^3 \frac{\varepsilon_{\text{au}} - 1}{\varepsilon_{\text{au}} + 2}, \quad \alpha_{\text{au},m} = \frac{r^5}{30} \left(\frac{\omega}{c}\right)^2 (\varepsilon_{\text{au}} - 1). \quad (\text{S24})$$

Meanwhile, we obtain the electric dipole moment contributions to radiative heat transfer by changing the magnetic polarizability tensor and magnetic Green's function in Eqs. (S14,S15) to their electric counterparts.

S4. DYADIC GREEN'S FUNCTION

In this section, we provide the expressions for the dyadic Green's function. The dyadic Green's function can be separated into the free space part and the reflected part $\bar{\bar{G}} = \bar{\bar{G}}^0 + \bar{\bar{G}}^r$. The free space part is [15],

$$\bar{\bar{G}}_m^0(\vec{r}_i, \vec{r}_j, \omega) = \bar{\bar{G}}_e^0(\vec{r}_i, \vec{r}_j, \omega) = \frac{e^{ik_0 D}}{4\pi D} \left[\left(1 + \frac{ik_0 D - 1}{k_0^2 D^2}\right) \bar{\bar{I}}_3 + \frac{3 - 3ik_0 D - k_0^2 D^2}{k_0^2 D^2} \frac{\bar{\bar{D}}\bar{\bar{D}}}{D^2} \right], \quad (\text{S25})$$

where $\bar{\bar{D}} = \vec{r}_i - \vec{r}_j$, and the subscript m, e denotes the magnetic and electric Green's functions. The reflected part of Green's function is [15],

$$\bar{\bar{G}}_m^r(\vec{r}_i, \vec{r}_j, \omega) = \frac{i}{8\pi^2} \int \frac{d\vec{q}}{k_z} e^{i\vec{q}(\vec{r}_i - \vec{r}_j)} e^{ik_z(z_i + z_j)} \left(\frac{r_p}{q^2} \begin{bmatrix} q_y^2 & -q_x q_y & 0 \\ -q_x q_y & q_x^2 & 0 \\ 0 & 0 & 0 \end{bmatrix} + \frac{r_s}{k_0^2 q^2} \begin{bmatrix} -q_x^2 k_z^2 & -q_x q_y k_z^2 & -q_x k_z q^2 \\ -q_x q_y k_z^2 & -q_y^2 k_z^2 & -q_y k_z q^2 \\ q^2 q_x k_z & q^2 q_y k_z & q^4 \end{bmatrix} \right), \quad (\text{S26})$$

$$\bar{\bar{G}}_e^r(\vec{r}_i, \vec{r}_j, \omega) = \frac{i}{8\pi^2} \int \frac{d\vec{q}}{k_z} e^{i\vec{q}(\vec{r}_i - \vec{r}_j)} e^{ik_z(z_i + z_j)} \left(\frac{r_s}{q^2} \begin{bmatrix} q_y^2 & -q_x q_y & 0 \\ -q_x q_y & q_x^2 & 0 \\ 0 & 0 & 0 \end{bmatrix} + \frac{r_p}{k_0^2 q^2} \begin{bmatrix} -q_x^2 k_z^2 & -q_x q_y k_z^2 & -q_x k_z q^2 \\ -q_x q_y k_z^2 & -q_y^2 k_z^2 & -q_y k_z q^2 \\ q^2 q_x k_z & q^2 q_y k_z & q^4 \end{bmatrix} \right), \quad (\text{S27})$$

where \vec{q} is the in-plane wavevector, $k_z = \sqrt{k_0^2 - q^2}$, z_i, z_j are the distance between \vec{r}_i, \vec{r}_j and the niobium slab interface, and r_s, r_p are the Fresnel reflection coefficients. In the near-field, Green's function is commonly dominated by evanescent wave contributions with momentum $q \gg k_0$. Therefore, $\bar{\bar{G}}_m^r$ will be dominated by the r_s term in Eq. (S26), while $\bar{\bar{G}}_e^r$ will be dominated by the r_p term in Eq. (S27).

-
- [1] S.-A. Biehs, R. Messina, P. S. Venkataram, A. W. Rodriguez, J. C. Cuevas, and P. Ben-Abdallah, *Reviews of Modern Physics* **93**, 025009 (2021).
 - [2] R. Messina, M. Tschikin, S.-A. Biehs, and P. Ben-Abdallah, *Physical Review B* **88**, 104307 (2013).
 - [3] A. V. Pronin, M. Dressel, A. Pimenov, A. Loidl, I. V. Roshchin, and L. Greene, *Physical Review B* **57**, 14416 (1998).
 - [4] A. Gubin, K. Il'in, S. Vitusevich, M. Siegel, and N. Klein, *Physical Review B—Condensed Matter and Materials Physics* **72**, 064503 (2005).
 - [5] O. Klein, E. Nicol, K. Holczer, and G. Grüner, *Physical Review B* **50**, 6307 (1994).
 - [6] D. C. Mattis and J. Bardeen, *Physical Review* **111**, 412 (1958).
 - [7] R. Pöpel, *Journal of applied physics* **66**, 5950 (1989).
 - [8] L. Mattheiss, *Physical Review B* **1**, 373 (1970).
 - [9] M. Dressel, *Advances in Condensed Matter Physics* **2013**, 104379 (2013).
 - [10] B. D. Cullity and C. D. Graham, *Introduction to magnetic materials* (John Wiley & Sons, 2011).
 - [11] R. D. Sanchez, J. Rivas, P. Vaquero, M. Lopez-Quintela, and D. Caero, *Journal of magnetism and magnetic materials* **247**, 92 (2002).
 - [12] M. Rajendran, S. Deka, P. Joy, and A. Bhattacharya, *Journal of Magnetism and Magnetic Materials* **301**, 212 (2006).
 - [13] A. H. Sihvola, *Optics letters* **19**, 430 (1994).
 - [14] F. Khosravi, W. Sun, C. Khandekar, T. Li, and Z. Jacob, *New Journal of Physics* **26**, 053006 (2024).
 - [15] L. Novotny and B. Hecht, *Principles of nano-optics* (Cambridge university press, 2012).